Collective optical properties of silver nanoparticles organized in two-dimensional superlattices

A. Taleb, V. Russier, A. Courty, and M. P. Pileni*
Laboratoire SRSI, URA 1662, Université Pierre et Marie Curie (Paris VI), Boîte Postale 52, 4 Place Jussieu, F.75231 Paris Cedex 05, France
and CEA-Saclay, DRECAM-SCM, F.911 91 Gif-sur-Yvette, France
(Received 20 April 1998; revised manuscript received 6 October 1998)

In this paper we describe collective properties of silver nanoparticles organized in two-dimensional superlattices. Our aim is to show that we can control the state of organization of the silver particles deposited on the substrate. Then the particles are found in the form of either a well-organized two-dimensional array of isolated particles or disordered and coalesced particles distributed more or less randomly on the surface. The optical spectra are compared with both polarized and unpolarized light. When particles are arranged in a hexagonal array, an asymmetrical and broad peak is observed. Under *p*-polarized light, a new high-energy peak appears that is interpreted as a collective effect, resulting from the mutual interactions between particles. We support this conclusion from numerical calculations performed on finite-size clusters of silver spheres, where only the electrodynamic interactions between the spheres are taken into account. With disordered and coalesced system the high-energy peak disappears whereas a peak toward low energy is observed. This is attributed to coalesced particles. [S0163-1829(99)12415-9]

I. INTRODUCTION

Well-defined, ordered solids prepared from tailored nanocrystallite building blocks provide opportunities for optimizing properties of materials and offer possibilities for observing interesting, new, and potentially useful collective physical phenomena. In the past few years, several techniques have been developed for directing the self-assembly of nanocrystals into ordered aggregates or quantum dots superlattices.[1–11] These assemblies present some very exciting possibilities. In principle, interparticle separations, particle size, and particle stoichiometry may be individually controlled to produce a macroscopic solid with a tailored band structure. This is similar to the well-known case of a one-dimensional quantum dot superlattice that might be engineered to provide unique physical properties. Such materials could be important constituents of tunnel resonance resistors[12] in microelectronic devices.

Large classes of material can be produced by using reverse micelles as templates.[1–3] Several years ago, by using this technique, we demonstrated that nanosized silver metal particles can be obtained.[13] The particle size was controlled from 2 to 8 nm and the optical properties of these clusters confirm predictions based on simulations. To decrease the size distribution, a size selection precipitation method was used.[14] Particles were arranged either in monolayers organized in a hexagonal network, or in three-dimensional (3D) superlattices with a face-centered-cubic (fcc) structure.[14] Similar arrangements were obtained a few years ago with silver sulfide nanoparticles.[15–17] By using different preparation modes, several groups have succeeded in forming patterns with gold and silver nanosized particles.[18–24] We previously compared the optical properties of nanosized silver particles dispersed in hexane solution and self-assembled in 2D or 3D networks.[25]

In this paper, the optical properties of silver particles deposited on a cleaved graphite substrate organized or not in 2D superlattices are presented. A peak toward high energy compared to that of isolated particles is observed. It disappears when particles are either disordered and coalesced. In order to explain qualitatively this optical response numerical calculations of the extinction cross section for finite-size clusters of spherical silver particles are presented.

II. EXPERIMENT

A. Products

AOT was purchased from Sigma. Isooctane, hexane, and pyridine were from Fluka. Hydrazine and dodecanethiol were obtained from Prolabo (France) and Janssen chemicals, respectively. The materials were not purified any further. Silver di(2-ethyl-hexyl) sulfosuccinate, Ag(AOT), was prepared as described previously.[26] The graphite substrate highly oriented pyrolytic graphite (HOPG) were obtained from Carbon Loraine (France).

B. Optical measurements and characterization

Measurement of the optical spectra have been performed on a conventional Varian Cary I spectrophotometer equipped with rotational stages for angular measurement in the energy interval $1.9 < E < 4.9$ eV. The polarization of the light can be perpendicular (*s*) or parallel (*p*) to the plane of incidence and the angle of incidence can range from 15° to 60° with respect to the surface normal. For particles in solution, absorption spectra were recorded in 2-mm cuvettes. For particles deposited on a cleaved carbon graphite substrate, the difference reflectance ΔR between the substrate with the particles on its surface and the clean substrate has been measured. The bandwidth have been measured at half-maximum by taking the minimum at low energy (approximately 2 eV) as a reference for the zero of the spectra. The transmission electron microscope (JEOL 100CX) operates at 100 kV. The mean di-

ameter D_m and the standard deviation σ_m were derived from an average number of 500 particles.

III. MODELIZATION AND CALCULATION OF THE OPTICAL SPECTRA OF SILVER NANOPARTICLES

In this section we consider silver nanoparticles coated with dodecanethiol. They are either dispersed in a solvent as hexane and considered as isolated particles or organized on a graphite substrate in a 2D hexagonal network. We calculate the optical properties of these particles either dispersed in a solvent or organized on a substrate.

The absorption spectrum of isolated spherical particles is characterized by the well-known Mie resonance,[28–30] occurring at a frequency ω_0 such that

$$\varepsilon_{1s}(\omega_0) = -2\varepsilon_m, \tag{1}$$

where $\varepsilon_s(\omega) = \varepsilon_{1s}(\omega) + i\varepsilon_{2s}(\omega)$ is the dielectric function of the silver spherical particles and ε_m is the dielectric function of the surrounding medium. Because the particles are coated by the dodecanethiol and the particles are dispersed in hexane, the dielectric constant can be assumed to be $\varepsilon_m = 2$. As matter of fact the dielectric constants of dodecane and hexane solvent are 1.98 and 1.88, respectively. The full half-width of the resonance peak is determined by the imaginary part and also by the slope of the real part of the dielectric function at the frequency ω_1. For randomly oriented ellipsoidal particles, the optical response can be interpreted in terms of the depolarization factors. The optical spectrum is characterized by two resonance peaks corresponding to the polarisabilities along the major and the minor axes.[31–34,36–38]

The optical response of isolated spherical particles coated by an alkyl chain (dodecanethiol) deposited on a substrate with a rather small distance of closest approach is investigated. The optical absorption spectra are deduced from numerical calculations on clusters of silver spheres by using the framework of available calculations.[39–43] In first approximation, we focus on the effect of the mutual electrodynamic interactions between the particles separated by a given distance. Furthermore, the substrate is not taken into account. We consider finite-size clusters including N_t metallic spheres of radii R_i located at positions r_i and the extinction cross section σ_e is calculated. The absorbance A can be related to σ_e according to

$$A = -\log_{10}(1 - \rho\sigma_e), \tag{2}$$

where ρ is the density of metallic particles per unit area.[34–36] Here, avoiding the determination of ρ, the present results are explained in terms of $\ln(\sigma_e)$ which presents a similar behavior as A, in particular concerning the resonance peak structure. In order to take into account the presence of the coating molecules at the surface of the metal spheres, the cluster may be immersed in an homogeneous medium of dielectric constant $\varepsilon_m \neq 1$. The metal spheres are characterized by an uniform and local dielectric function $\varepsilon_s(\omega)$. In this work, we take ε_s from the Drude approximation:

$$\varepsilon_s(\omega) = \varepsilon_b - \omega_{p0}^2/[\omega(\omega + i\tau)], \tag{3}$$

where ω_{p0}, ε_b, and τ are the free electron plasmon resonance, the polarizability due to the d electrons and the relaxation time, respectively. ε_b can be considered as a constant for silver at the frequencies that we consider ($\hbar\omega < 4.5$ eV), and is fitted in such a way that the bulk plasmon frequency, $\omega_p = \omega_{p0}/\varepsilon_b^{1/2}$ coincide with the experimental value, $\omega_p = 3.8$ eV.[44] The relaxation time τ is corrected to take into account the finite size of the spheres in the standard way,[39,45]

$$1/\tau = 1/\tau_0 + v_F/R, \tag{4}$$

where τ_0 and ν_F are the value for the infinite system and the Fermi velocity, respectively. This particle size correction is only approximate, but this is sufficient for the present calculation since our aim here is not a precise determination of the width of the resonance peaks. Moreover, this one is in any case greatly affected by the chemical species adsorbed at the surface of the particles, an effect that cannot be taken into account through a simple correction like Eq. (4). Notice that the correction (4) does not affect the position of the resonance, and only widens the peaks. The magnetic susceptibility of the spheres is $\mu = 1$. The incident electromagnetic field is a plane wave of wave vector $\mathbf{k}$ and frequency ω. Inside the spheres, the wave vector is complex and of amplitude $k_s = (\omega/c)(\varepsilon_s)^{1/2}$.

The calculation of the extinction cross section is done in the framework of the method given by Gérardy and Ausloos[43] and is described in the Appendix (see below). It is found that

$$\sigma_e = -\left[\pi \sum_{i=1,N} (kR_i)^2\right]^{-1} \times \mathrm{Re}\left\{\sum_{i=1,N} \sum_{q,p} \left(a^*_{qp}(i)c_{qp}(i) + b^*_{qp}(i)d_{qp}(i)\right)\right\}. \tag{5}$$

In the following, the normal to the surface is the z axis, the surface defines the (x,y) plane and the plane of incidence is the (x,z) plane. The wave vector of the incident wave is defined by the three Euler angles β, θ, and γ (Fig. 1). The angle β defines the orientation of $\mathbf{k}$ with respect to a fixed direction in the surface plane (we take $\beta = 0$ for $\mathbf{k}_y = 0$), θ coincides with the incident angle, and γ defines the polarization of the incident electric field: $\gamma = 0$ and $\gamma = \pi/2$ correspond to the p and to the s polarizations, respectively.

In order to use the calculations performed on finite-size clusters for the description of actual infinite two-dimensional systems, we must take care of both the shape and size effects on the results of the calculations. Concerning the shape effect we find that a spurious anisotropy of the optical response in the (x,y) plane is obtained if the symmetry of the cluster does not respect the symmetry of the whole lattice we model. Therefore, in the present calculations, we use only clusters

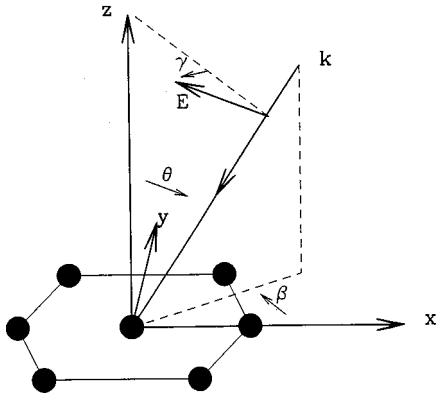

FIG. 1. Coordinate system used in the calculation. The solid circles represent the center of an hexagonal cluster.

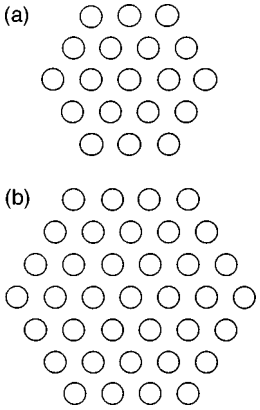

FIG. 2. Clusters used in the calculations (a) and (b) correspond to the hexagonal structure (see text for details)

symmetric with respect to a rotation of angle $\pi/3$ and axis z to represent the two-dimensional hexagonal lattice. Avoiding the finite-size effects is more complicated. As we shall see below, the spectra are characterized by two main resonance modes ω_- and ω_+; let us denote by $\Delta\omega$ the shift $(\omega_+ - \omega_-)$. Assuming that the leading contribution of this effect is due to the long-range dipolar interactions between the dipoles induced in the polarizable spheres by the local field, we find that the shift $\Delta\omega$ behaves as

$$\Delta\omega(\lambda,N)=\Delta\omega(\lambda,\infty)-f(\lambda)/N^{1/2}, \tag{6}$$

where $\lambda=(2R/d)^3$ and f, determined by the sum of the polarization fields created by all the induced dipoles, depends only on λ. For a given value of λ we can then estimate the correction $[\Delta\omega(\lambda,\infty)-\Delta\omega(\lambda,N_1)]$ by using the results $\Delta\omega(\lambda,N_1)$ and $\Delta\omega(\lambda,N_2)$ calculated on two clusters of different sizes, N_1 and N_2, provided that N_1 and N_2 are sufficiently large. We get

$$\Delta\omega(\lambda,\infty)=\Delta\omega(\lambda,N_1)+[(\Delta\omega(\lambda,N_1)-\Delta\omega(\lambda,N_2))/(N_2{}^{-1/2}-N_1{}^{-1/2})^{-1}]/N_1{}^{1/2}. \tag{7}$$

From the numerical calculation, we find that limiting the multipole expansion to $l_s=2$ is sufficient, the same results are obtained when we compare the calculated absorption spectrum with either $l_s=2$ or $l_s=4$. Notice that the expansion limited to $l_s=2$ is so accurate partly because the particles are not nearly at contact. The clusters that we consider are mainly 19 particles clusters with a hexagonal structure and the size effect has been estimated, according to Eq. (7), from calculations on 37 particles clusters. The clusters are shown in Fig. 2. The interparticle distance is $d=2R+\Delta$, where Δ is the minimum spacing between particles and is independent of R ($\Delta=1.85$ nm). Concerning the diameter of the particles we take $2R=5.30$ or 6.60 nm. The external medium dielectric constant, is chosen close to that of the alkyl chain used to coat the particles ($\varepsilon_m=2$). The cross section σ_e for particles of diameter $2R=6.60$ nm, interparticle distance $d=7.15$ nm and $\varepsilon_m=2$ as calculated with a 19-particle cluster is shown in Fig. 3 for the s and p polarizations, respectively. The main features of the spectra are first that we get two resonances at frequencies ω_- and ω_+ with $\omega_-<\omega_0<\omega_+$, and second that the s-polarization spectrum presents only a single peak at $\omega=\omega_-$ while the p-polarization spectrum presents both peaks, the amplitude of the high-energy one being an increasing function of the angle of incidence. Such a behavior is clearly the result of the optical anisotropy of the system; namely, its polarizability takes a different value in the direction normal to the surface, and in a direction parallel to the surface (for the lattice considered the system is isotropic in the surface plane). This anisotropy is exhibited in the p-polarization case since then the incident electric field has a component parallel, E_x, and a component normal, E_z, to the surface, while in the s-polarization case the electric field has only a component parallel to the surface, E_y. For the smaller particles ($2R=5.30$ and $d=7.15$ nm), the absorption spectra are similar, with a smaller value for the shift $\Delta\omega$, due to a smaller value of the parameter λ. The results for the resonance frequencies are given in Table I.

IV. SYNTHESIS OF SILVER NANOPARTICLES

The silver nanoparticles are synthesized in water droplets in oil stabilized by a monolayer of surfactant.[1,3] This colloidal dispersion is usually called reverse micelles and the surfactant used is sodium bis(2 ethyl-hexyl) sulfosuccinate designated Na(AOT). The diameter of the water droplets varies linearly, from 0.5 to 18 nm,[1] with the water to surfactant concentration ratio. When two droplets, one containing hydrazine as a reducing agent and the other Ag^+, are in contact, they form a dimmer which induces a reduction reaction.[13] Immediately after mixing these two reverse micellar solutions, $(Ag)_n$ nanoparticles are formed. Such syntheses are performed at various droplet sizes. Particles kept a long time in reverse micelles flocculate and remain in the bottom of the vessel. To prevent such effect, dodecanethiol is added to micellar solution containing $(Ag)_n$ nanoparticles. A selective reaction with the silver atoms at the surface of the particles takes place. To remove the surfactant, ethanol is added to the micellar solution. This induces flocculation of dodecanethiol coated particles. The precipitate is then dispersed in hexane. The size and shape of particles obtained by

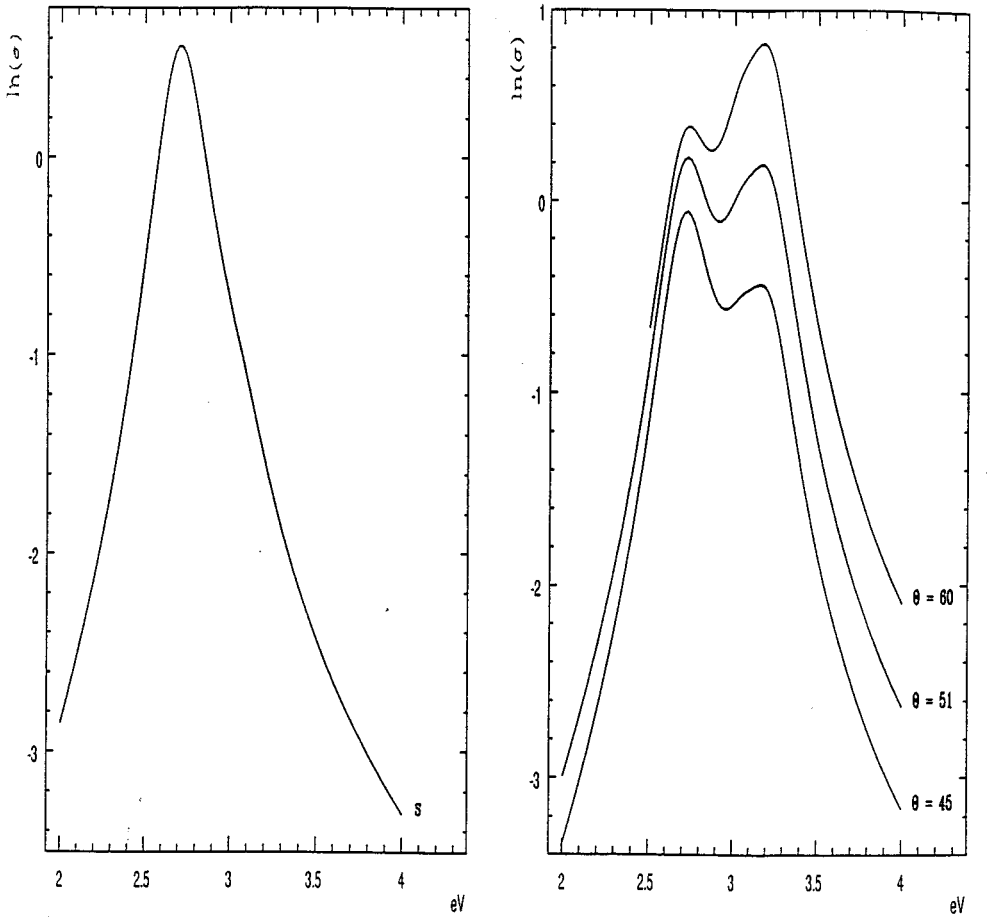

FIG. 3. Extinction cross section for the cluster of Fig. 2(b); $2R=6.60$ nm, $d=8.45$ nm, $\varepsilon_m=2$, for both s and p polarizations. In this later case, the angle of incidence, in degrees is indicated.

using this procedure differ with the amount of dodecanethiol added and with the delay before the extraction process takes place.

At this point of the procedure, various approaches are taken. (i) Syntheses are made in water droplets having 0.6 nm as average diameter. Immediately after mixing the two micellar solutions, $(Ag)_n$ nanoparticles are formed. Three different procedures are used: (1) Immediately after synthesis, the particles are coated with a very small amount of dodecanethiol (0.5 μl/ml) and extracted from micelles and then dispersed in hexane. After 24 h, the particles flocculate and those left on the bottom of the vessel are deposited on the substrate. The transmission electron microscopy (TEM) pattern [Fig. 4(a)], shows isolated nanoparticles with 5 nm average size and 17% polydispersity. Some amount of coalesced particles are observed in part of the copper grid recovered by cleaved carbon. (2) Immediately after synthesis, 2 μl/ml of dodecanethiol is added to the reverse micelles and the coated particles are immediately extracted from reverse micelles and then dispersed in hexane. A size selection takes place. The average diameter of the particles is 5 nm with a rather low size distribution (15%). The particles are highly stable. By deposition on a cleaved carbon substrate, a self-organization in a hexagonal compact network [Fig. 4(c)] is observed.

TABLE I. Energy resonance obtained from the extinction cross sections calculated on the clusters with hexagonal structure. The shift $\Delta\omega$ for the infinite surface is deduced using Eq. (7).

N	$2R$ (nm)	d (nm)	ε_m	ω_- (eV)	ω_+ (eV)	$\Delta\omega$ (eV)
19	5.30	7.15	1	3.14	3.40	0.26
19	5.30	7.15	2	2.77	3.10	0.33
19	6.60	8.45	1	3.12	3.42	0.30
19	6.60	8.45	2	2.72	3.16	0.44
37	6.60	8.45	2	2.67	3.20	0.53
37	6.60	8.45	1	3.10	3.43	0.33
∞	5.30	7.15	2			0.51
∞	6.60	8.45	2			0.76

(ii) For droplets having 12 nm as average diameter, the average $(Ag)_n$ size is 3.4 nm with a rather large size distribution (43%). Dodecanethiol (1 μl/ml) is then added to the micellar solution. The particles are extracted from the micelles as described above. To reduce the size distribution, a size selected precipitation process, as described in detail in our previous paper,[14] is used: pyridine is progressively added to hexane solution containing the silver coated particles. At a given volume of added pyridine (roughly 50%), the solution becomes cloudy and a precipitate appears indicating agglomeration of the largest particles. The solution is centrifugated and an agglomerated fraction rich in large particles is collected, leaving the smallest particles in the supernatant. The precipitate, dispersed in hexane, forms a homogeneous clear solution. By repeating the same procedure several times,

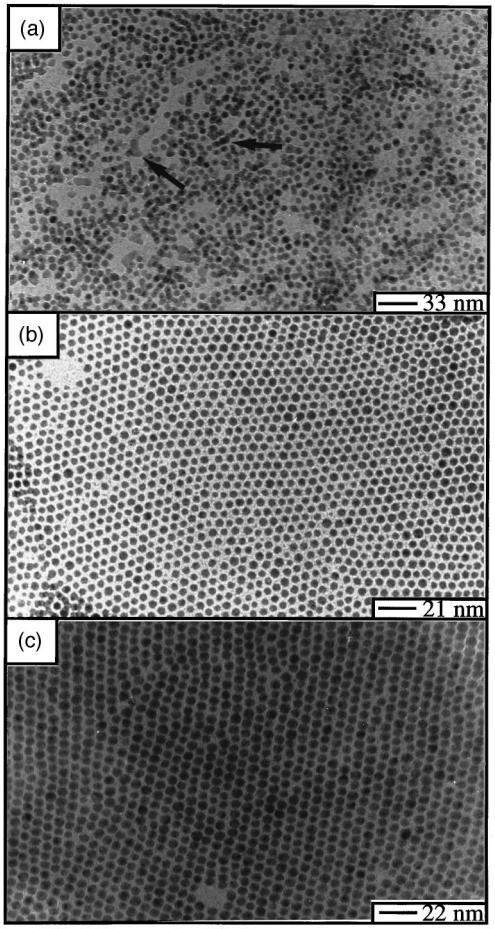

FIG. 4. TEM patterns of particles I (a), II (b) 4 nm, and III (c) 5 nm.

4-nm silver nanoparticles with a rather low size distribution (13%) are obtained. By deposition of the particles dispersed in hexane on a copper grid covered by cleaved carbon, a self-organization in a hexagonal network is observed [Fig. 4(b)].

By using these various procedures, it is possible to obtain particles having an average size of either 4 or 5 nm with a low size distribution and arranged in a hexagonal network after deposition on a carbon grid, [Figs. 4(b) and 4(c)] or isolated and/or coalesced particles [Fig. 4(a)]. To simplify the text, the various particles will be referred to as particles I [Fig. 4(a)], II [Fig. 4(b)], and III [Fig. 4(c)], respectively. In first approximation we consider that particles II and III are spherical. This is consistent with the TEM patterns. The number of silver atoms on a carbon grid is evaluated by assuming an average size and by counting more than 500 particles. On average the number of silver atoms deposited on the grid remains at approximately $50/\text{nm}^2$.

V. OPTICAL PROPERTIES OF SILVER NANOPARTICLES ARRANGED OR NOT IN 2D SUPERLATTICES

From the syntheses described above, it is clearly shown that the particles differ by their size and shape. We choose to separate them into two classes: (i) Particles I [Fig. 4(a)] are not ordered on the substrate. The size and the shape of particles I are mainly spherical and isolated on the substrate.

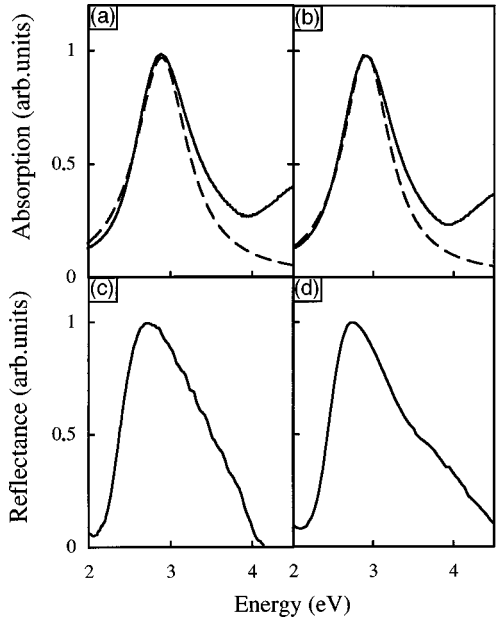

FIG. 5. Absorption spectra normalized to unity of particles II and III dispersed in hexane (a) and (b), and reflectance spectra of these particles deposited on the substrate under unpolarized light (c) and (d).

However, some of them are close together or coalesced [see arrow in Fig. 4(a)]. (ii) Particles II and III are, in first approximation, spherical with a very low size distribution. They are organized, all over the substrate, in a hexagonal network. The average distance between particles is 1.8 nm. From the TEM grid, no coalesced particles are observed [Figs. 4(b) and 4(c)]. When they are dispersed in a solvent they are considered as isolated particles.

In the following we present the optical properties of either particles dispersed in a solvent or deposited on a substrate. In the case of particles deposited on the substrate we first consider particles I and then particles II and III.

A. Isolated spherical particles

The optical response of particles II [Fig. 5(a)] and particles III [Fig. 5(b)] dispersed in hexane are characterized by well-defined plasmon peak centered at 2.9 eV. The simulated spectra (dashed line) indicate that the resonance peak is close to a Lorentzian [Fig. 5(a) and 5(b)]. The misfit observed at the high energy is due to the interband transitions $(4d\text{-}5sp)$.[27] Such an optical response has been well described by the quasistatic approximation of the Mie theory,[28–29] where the optical extinction cross section is given mainly by the dipole absorption and shows a narrow plasmon resonance influenced by the contribution of the interband transitions. Table II shows an increase in the bandwidth with decreasing the particle size. This has been well established in these decades.[29,39] It is attributed to a decrease in the electronic mean free path for the smaller particles and monitored by the imaginary part and the slope of the real part of the dielectric function at the frequency ω_1. From Eqs. (1) and (3) [used for silver with $\varepsilon_m = 2$ for hexane solution] [see Sec. III), the peak position ($\omega_0 = 2.95\,\text{eV}$) is found to be similar to that obtained from experimental data [Figs. 5(a) and 5(b)].

TABLE II. Maximum of the plasmon peak and average bandwidth obtained with nonpolarized light, E_{max} and ΔE, *s* polarized light, $E^{(s)}_{max}$ and $\Delta E^{(s)}$, and *p*-polarized light, $E^{(e)}_{max}$. All energies are in eV. (*a*) particles dispersed in solution; (*b*) particles deposited on the substrate.

Particles	I *b*	II *a*	II *b*	III *a*	III *b*
E_{max}		2.9	2.7	2.9	2,7
$E^{(s)}_{max}$	2.7		2,9		2.9
$E^{(p)}_{max}$	2.7–3.1		2.8–3.8		2.8–3.8
ΔE		0.8 ± 0.05	1.1 ± 0.05	0.7 ± 0.05	1.0 ± 0.05
$\Delta E^{(s)}$			1.2 ± 0.05		0.8 ± 0.05

B. Optical properties of nonspherical particles deposited on a substrate in a disordered way (particles I)

To investigate the presence of several resonance peaks, the reflective spectra under polarized light perpendicular (*s*) or parallel (*p*) to the plane of incidence at various incident angles θ are recorded. Under *s* polarization, the electric field vector is always directed along the major axis of the spheroidal particles [parallel to the substrate]. This tends to be insensitive to plasmon mode oriented perpendicular to the substrate[35] and does not provide any information on the optical surface anisotropy. Conversely, under *p* polarization, the electric field has two components: One is along the minor axis growing with increasing the θ angle. The second one is along the major axis and decreases with increasing the θ angle. Hence, the (*p*) polarization provides information on the optical film anisotropy.[32]

Under *s* polarization, the optical spectra obtained at various θ angles [Fig. 6(a)] show one resonance peak at 2.7 eV. This is attributed to the surface plasmon parallel to the substrate. Conversely, under *p* polarization [Fig. 6(b)], a splitting of the optical spectra with increasing θ angle is observed: one of the peak is shifted toward high energy compared to that of isolated spherical particles whereas the second one is at lower energy.

Figure 4(a) shows that most of the particles keep similar size. However, it can be observed that, in some part of the TEM pattern, some particles form chains that are either close together or coalesced [see arrow on Fig. 4(a)]. Taking into account the TEM pattern, the optical behavior is explained as follows: Under *s* polarization the longitudinal surface plasmon mode is investigated whereas under the *p* polarization the longitudinal and transversal mode are explored. However under *p* polarization and low θ value, the contribution of longitudinal mode is higher than the transversal one. This explains why under *s* and *p* polarization at low θ value only one resonance peak is observed. In the present case, the maximum is found centered at 2.7 eV. This value is shifted toward low energy compared to that of the isolated spherical particles (2.9 eV). Such shift corresponds to a deviation of the shape compared to spheres. More the particles are anisometrical, more the shift toward low energy is enhanced.[40] On increasing θ value under *p* polarization, the contribution of transversal mode increases and induces the appearance of a new resonance peak which is shifted toward high energy compared to that of isolated spherical particles. Hence the presence of the two plasmon modes [Fig. 6(b)] indicates an optical anisotropy due to the non spherical shape of the particles as shown on a TEM grid [Fig. 4(a)].

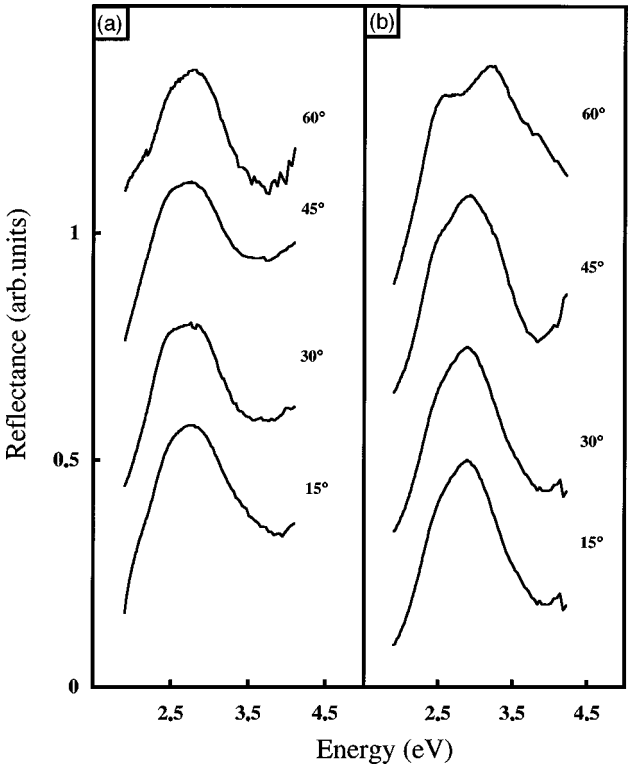

FIG. 6. Reflectance spectra of particles I under perpendicular (a) and parallel (b) polarized light at various incident angles θ.

C. Optical properties of spherical particles organized in 2D superlattices

Figures 5(c) and 5(d) show the optical spectra under unpolarized light of particles II and III deposited on graphite substrate and organized in hexagonal network. Their maximum is centered at 2.7 eV. In both cases, the optical spectra are shifted toward low energy compared to that of particles dispersed in hexane (2.9 eV). Conversely to what is observed for isolated particles [Fig. 5(a) and 5(b)], the optical spectra are asymmetrical. An increase in the bandwidth (1.1 and 1 eV, respectively) compared to isolated particles (0.8 and 0.7 eV) is observed. By washing the substrate, the absorption spectra of particles II and III dispersed in hexane are similar to those observed for isolated spherical particles. This indicates that the coated particles do not coalesced after deposition. The increase in the bandwidth compared to that observed for isolated particles has already been observed with silver particles randomly deposited on a glass substrate. The lack of symmetry observed can be attributed to additional resonance when particles are organized in a hexagonal network.

Under *s* polarization, the optical spectra of particles II and III (Fig. 7), recorded at various incident angles θ do not change with increasing θ. They are characterized by a maximum centered at 2.9 eV which is similar to that observed for isolated particles (Table II). However, the plasmon resonance peak remains asymmetric as observed under unpolarized light [Figs. 5(c) and 5(d)].

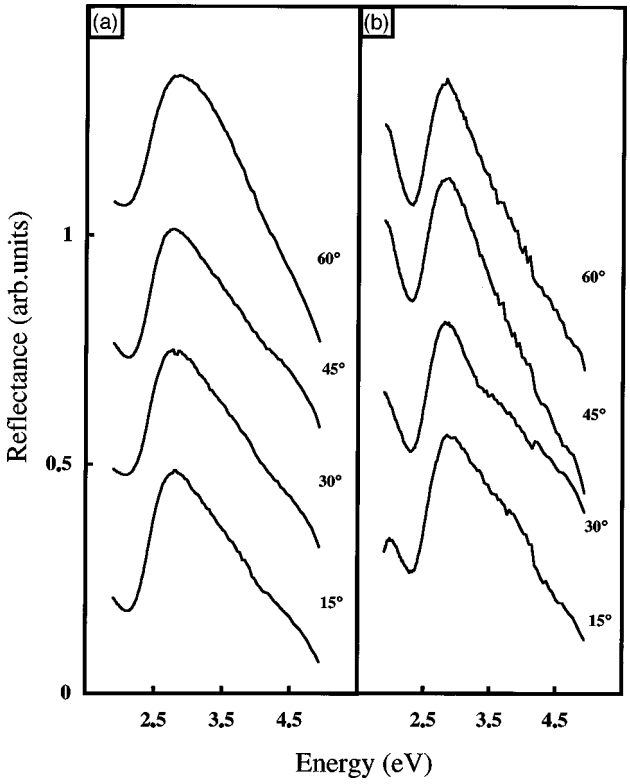

FIG. 7. Reflectance spectra of samples II (a) and III (b) obtained with *s*-polarized light at various incident angles θ.

Under *p* polarization, the optical spectra of particles II and III markedly change with the incident angle θ (Fig. 8): At low θ angle, one peak is observed. On increasing θ, a new plasmon resonance peak appears at high energy (Fig. 8). The

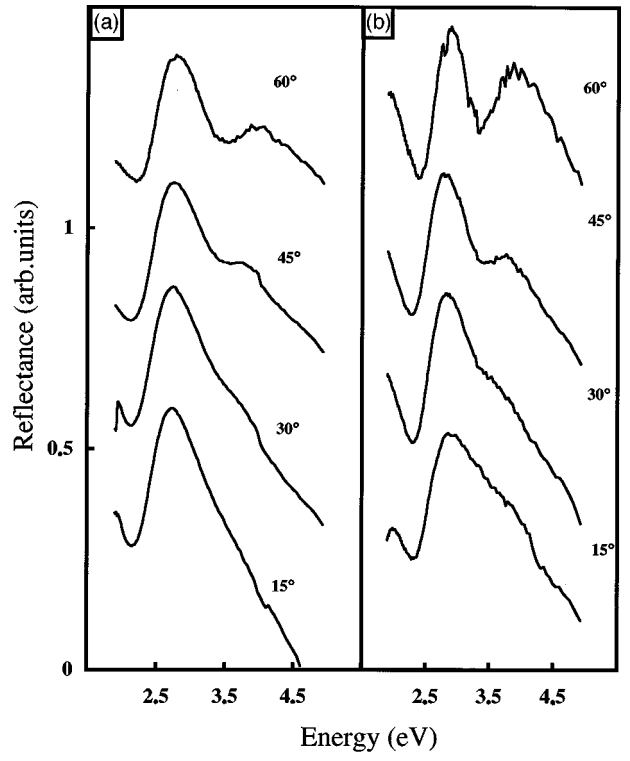

FIG. 8. Reflectance spectra of particles II (a) and III (b) obtained with *p*-polarized light at various incident angles θ.

comparison between the relative intensity peak indicates that the high-energy peak increases with increasing the particle size [Fig. 8(a), particles II (4 nm); Fig. 8(b), particles III (5 nm)]. At $\theta = 60°$, the two peaks are well defined: One is centered at 2.8 eV (ω_-) [close to that observed for isolated particles, ($\omega_0 = 2.9$ eV)] whereas the other one is centered at 3.8 eV (ω_+). Hence, when particles are organized in a hexagonal superlattice with 1.8 nm as average distance between particles, a new resonance peak appears at high energy whereas that one ($\omega_- = 2.8$ eV) close to that of isolated spherical particles ($\omega_0 = 2.9$ eV) still remains. These data are highly reproducible and do not depend on coverage defects. [This is because the excitation wavelength is large compared to the particle size and to the defects of the particle monolayer. Furthermore, the beam is rather broad. Hence, the optical response take into account the overall surface].

The comparison between the optical properties of particles deposited on the same substrate [cleaved graphite] and differing by their organizations [particles II and III form 2D superlattices whereas particles I are either isolated or coalesced] permits to conclude that the appearance of the resonance peak at 3.8 eV is due to the self-organization of the particles in a hexagonal network. This can be interpreted in terms of mutual interactions between particles. The local electric field results from dipolar interactions induced by particles at a given distance between each others. Near the particles, the field consist of the applied field plus a contribution due to all other dipoles and their images. The calculation on finite-size clusters shown in Sec. III gives, at a qualitative level, a correct explanation concerning the difference between the *s*- and the *p*-polarization spectra (Fig. 3): Under *s* polarization one resonance peak is observed whereas under *p* polarization an additional peak toward high energy appears. As observed in the experimental data shown in Fig. 8, the intensity of high energy peak increases with increasing the incidence angle.

Some discrepancies between the experimental and the calculated data can be listed as follows: (i) the absolute value of the low-energy resonance peak, ω_-, is 0.3 eV lower than that determined from the experiments ($\omega_- = 2.8$ eV). Conversely, for isolated spherical particles, a good correlation of the resonance frequency, between calculation ($\omega_0 = 2.95$ eV) and experimental ($\omega_0 = 2.9$ eV) data is obtained. The calculated value for ($\omega_+ - \omega_0$) is comparable to that for ($\omega_0 - \omega_-$) while in the experiment ω_- is very close to ω_0. (ii) The shift between the two resonance peaks, $\Delta\omega$, is underestimated by nearly a factor of 2.

These discrepancies between the experimental data and the calculation could be due to the following. (a) The fact that, in first approximation, the particles are assumed to be spherical. In fact, it has been demonstrated that the silver nanocrystals are faceted.[22] This could enhance the optical anisotropy. (b) We did not take into account the substrate effect. Although, for spherical particles, we do not expect an important change of the shift ($\omega_+ - \omega_-$) due to the substrate[37,38] the dielectric discontinuity due to the substrate leads to a shift in the resonance peak frequencies.[36–38] On the other hand, the substrate may introduce additional changes in the position of the frequencies through specific interactions with the particles and/or the chains of the molecules coating the particles.

We do not invoke either the interband transition or the bulk plasmon resonance in order to explain the high-energy peak observed at 3.8 eV in the particles II and III that disappears with the particles I because these two effects are characteristic of the bulk material and therefore should depend neither on the state of polarization nor on the shape of the particle. The calculation of the plasmon resonance of small metal particles including the bulk plasmon resonance has been performed by Ruppin and this latter resonance leads to a peak of very small amplitude that does not depend on the direction of the incident field.[42]

VI. CONCLUSION

Marked changes in the optical properties of silver nanoparticles deposited on graphite substrate and organized in 2D superlattices are observed. A high-energy resonance peak appears under p polarization and is attributed to the collective effect in term of mutual interaction between particles. As matter of fact, this high energy peak disappears when particles are either isolated or coalesced. The calculations taking into account interactions between particles permit to explain, qualitatively, such behavior. However, the particle-substrate interaction cannot be excluded.

APPENDIX

The calculation of the extinction cross section is done in the framework of the method given by Gérardy and Ausloos.[43] We do not consider longitudinal fields, since the dielectric function in the metallic spheres is local, and thus the electric and magnetic fields, E and H, respectively, are expanded on the sets of vectors $\{\mathbf{m}_{qp,\sigma}(i)\}$ and $\{\mathbf{n}_{qp,\sigma}(i)\}$ defined in the reference frames of the spheres ($i=1,N$), in terms of the unit vectors $\mathbf{r},\boldsymbol{\theta},\boldsymbol{\varphi}$ of the corresponding spherical coordinates

$$q(q+1)^{1/2}\mathbf{m}_{qp,\sigma}(i) = ipz_{q,\sigma}(kr)(Y_q{}^p/\sin\theta)\boldsymbol{\theta} - z_{q,\sigma}(kr)\partial_\theta(Y_q{}^p)\boldsymbol{\varphi}, \tag{A1a}$$

$$q(q+1)^{1/2}\mathbf{n}_{qp,\sigma}(i) = q(q+1)[z_{q,\sigma}(kr)/(kr)]Y_q{}^p\mathbf{r} + [krz_{q,\sigma}(kr)]'/(kr)\partial_\theta(Y_q{}^p)\boldsymbol{\theta} + ip[krz_{q,\sigma}(kr)]'/(kr)(Y_q{}^p/\sin\theta)\boldsymbol{\varphi}, \tag{A1b}$$

where $r=|\mathbf{r}-\mathbf{r}_i|$, the $Y_l{}^m$ are the spherical harmonics, and $z_{q,\sigma}(kr)$ are spherical Bessel functions of either the first kind, j_q, if $\sigma=1$, or the third kind, $h_q{}^{(1)}$, if $\sigma=3$. The prime in Eq. (A1b) denotes the derivative with respect to the argument. In the region surrounding the spheres, referred to in the following as the medium, we write[43]

$$E_M = E_0\sum_{i=1,N}\sum_{q=1,\infty}\sum_{p=-q,q}\{c_{qp}(i)\mathbf{m}_{qp,3}(i) + d_{qp}(i)\mathbf{n}_{qp,3}(i)\} + E_0,$$
$$H_M = H_0\sum_{i=1,N}\sum_{q=1,\infty}\sum_{p=-q,q}\{d_{qp}(i)\mathbf{m}_{qp,3}(i) + c_{qp}(i)\mathbf{n}_{qp,3}(i)\} + H_0, \tag{A2}$$

where E_0 and H_0 are the incident electric and magnetic fields, respectively. Inside a sphere j we have

$$E(j) = E_0\sum_{q=1,\infty}\sum_{p=-q,q}\{a^I{}_{qp}(j)\mathbf{m}_{qp,1}(j) + b^I{}_{qp}(j)\mathbf{n}_{qp,1}(j)\}, \tag{A3}$$

$$H(j) = H_j\sum_{q=1,\infty}\sum_{p=-q,q}\{b^I{}_{qp}(j)\mathbf{m}_{qp,1}(j) + a^I{}_{qp}(j)\mathbf{n}_{qp,1}(j)\},$$

the amplitude of the magnetic field, H_j being related to that of the incident field by $H_j=-i(ck_s/\omega)E_0$. The incident electric and magnetic fields can be expanded on the vectors $\mathbf{m}_{qp,1}(j)$ and $n_{qp,1}(j)$ corresponding to any of the spheres, say, j, chosen arbitrarily:

$$E_0 = E_0\sum_{q=1,\infty}\sum_{p=-q,q}\{a_{qp}(j)\mathbf{m}_{qp,1}(j) + b_{qp}(j)\mathbf{n}_{qp,1}(j)\},$$
$$H_0 = H_0\sum_{q=1,\infty}\sum_{p=-q,q}\{b_{qp}(j)\mathbf{m}_{qp,1}(j) + a_{qp}(j)\mathbf{n}_{qp,1}(j)\}. \tag{A4}$$

The coefficients $c_{qp}(i)$ and $d_{qp}(i)$ for the fields E_M and H_M are then calculated in terms of the coefficients $a_{qp}(i)$ and $b_{qp}(i)$ relative to the incident fields from the boundary conditions satisfied at the surface of each sphere, namely, the continuity of the tangent fields

$$(E_M-E)x(\mathbf{r}-\mathbf{r}_i)=0,$$
$$(H_M-H)x(\mathbf{r}-\mathbf{r}_i)=0, \quad \text{for } |\mathbf{r}-\mathbf{r}_i|=R_i. \tag{A5}$$

In order to perform the calculations, we have to limit the value of the multipolar order taken into account, namely, $l \leq l_s$. Then, defining the vector $\mathbf{a}$ by the set of the coefficients $\{a_{qp}(i)\}_{i\leq N;\, q\leq s;\, p\leq q}$ and similarly the vectors $\mathbf{b}$, $\mathbf{c}$, and $\mathbf{d}$ from the corresponding coefficients, the solution for $\mathbf{c}$ and $\mathbf{d}$ can be written in a quite compact form, using a matrix notation[43]

$$\mathbf{c} = M_1{}^{-1}[\mathbf{a}+M_3\mathbf{b}],$$
$$\mathbf{d} = M_2{}^{-1}[\mathbf{b}+M_4\mathbf{a}], \tag{A6}$$

the important point in this equation being the fact that the matrices M_k are independent of the incident wave.

The extinction cross section σ_e is determined from the integral of the normal component of the Poynting vector on a large sphere including the whole cluster and is given (in unit of the surface of the particles) in terms of the expansion coefficients $a_{qp}(i)$, $b_{qp}(i)$, $c_{qp}(i)$, and $d_{qp}(i)$ (Ref. 43),

$$\sigma_e = -\left[\pi \sum_{i=1,N} (kR_i)^2\right]^{-1} \times \mathrm{Re}\left\{\sum_{i=1,N} \sum_{q,p} (a^*_{qp}(i)c_{qp}(i) + b^*_{qp}(i)d_{qp}(i))\right\}. \quad \text{(A7)}$$

*Author to whom correspondence should be addressed.

[1] M. P. Pileni, J. Phys. Chem. **97**, 6961 (1993).
[2] J. Fendler, and F. C. Meldrum, Adv. Mater. **7**, 607 (1995).
[3] M. P. Pileni, Langmuir **13**, 3266 (1997).
[4] K. Solecka-Cermakova, and B. Vickova, J. Phys. Chem. **100**, 4954 (1996).
[5] A. Badia, W. Gao, S. Singh, L. Demers, L. Cuccia, and L. Reven, Langmuir **12**, 1262 (1996).
[6] M. Brust, D. Bethell, D. J. Schiffrin, and C. J. Kiely, Adv. Mater. **7**, 795 (1995).
[7] J. P. Spatz, A. Roescher, and M. Moller, Adv. Mater. **8**, 337 (1996).
[8] N. Kimizuka and T. Kunitake, Adv. Mater. **8**, 89 (1996).
[9] A. S. Tse, Z. Wu, and S. A. Asher, Macromolecules **28**, 6533 (1995).
[10] S. A. Asher, J. Holtz, L. Liu, and Z. Wu, J. Am. Chem. Soc. **116**, 4997 (1994).
[11] S. Y. Chang, L. Liu, and S. A. Asher, J. Am. Chem. Soc. **116**, 6739 (1994).
[12] M. Giersig, and P. Mulvaney, Langmuir **9**, 3408 (1993).
[13] C. Petit, P. Lixon, and M. P. Pileni, J. Phys. Chem. **97**, 12 974 (1993).
[14] A. Taleb, C. Petit, and M. P. Pileni, Chem. Mater. **9**, 950 (1997).
[15] L. Motte, F. Billoudet, and M. P. Pileni, J. Phys. Chem. **99**, 16 425 (1995).
[16] L. Motte, F. Billoudet, E. Lacaze, and M. P. Pileni, Adv. Mater. **8**, 1018 (1996).
[17] L. Motte, F. Billoudet, E. Lacaze, J. Douin, and M. P. Pileni, J. Phys. Chem. **101**, 138 (1997).
[18] R. L. Whetten, J. T. Khoury, M. M. Alvarez, S. Murthy, I. Vezmar, Z. L. Wang, C. C. Cleveland, W. D. Luedtke, and U. Landman, Adv. Mater. **8**, 429 (1996).
[19] M. Brust, D. Bethell, D. J. Schiffrin, and C. J. Kiely, Adv. Mater. **7**, 9071 (1995).
[20] S. A. Harfenist, Z. L. Wang, M. M. Alvarez, I. Vezmar, and R. L. Whetten, J. Phys. Chem. **100**, 13 904 (1996).
[21] J. R. Heath, C. M. Khobler, and D. J. Leff, J. Phys. Chem. B **101**, 189 (1997).
[22] S. A. Harfenist, Z. L. Wang, R. L. Whetten, I. Vezmar, and M. M. Alvarez, Adv. Mater. **9**, 817 (1997).
[23] P. C. Ohara, J. R. Heath, and W. M. Gelbart, Angew. Chem. Int. Ed. Engl. **36**, 1077 (1997).
[24] W. D. Luedthe and U. Landman, J. Phys. Chem. **32**, 13 323 (1996).
[25] A. Taleb, C. Petit, and M. P. Pileni, J. Phys. Chem. B **102**, 2214 (1998).
[26] C. Petit, P. Lixon, and M. P. Pileni, Langmuir **7**, 2026 (1991).
[27] T. Yamaguchi, M. Ogawa, H. Takahshi, N. Saito, and E. Anno, Surf. Sci. **129**, 232 (1983).
[28] G. Mie, Ann. Phys. (Leipzig) **25**, 377 (1908).
[29] *Absorption and Scattering of Light by Small Particles*, edited by C. F. Bohren, and D. R. Huffman (Wiley, New York, 1983).
[30] S. Yoshida, T. Yamaguchi, and A. Kinbara, J. Opt. Soc. Am. **61**, 62 (1971); **61**, 463 (1971).
[31] R. Chauvaux and A. Meessen, Thin Solid Films **62**, 125 (1979).
[32] P. A. Bobbert and J. Vlieger, Physica A **147**, 115 (1987).
[33] M. M. Wind, P. A. Bobbert, J. Vlieger, and D. Bedeaux, Physica A **157**, 269 (1989).
[34] P. Royer, J. L. Bijeon, J. P. Goudonnet, T. Inagaki, and E. T. Arakawa, Surf. Sci. **217**, 384 (1989).
[35] (a) S. W. Kennerly, J. W. Little, R. J. Warmack, and T. L. Ferrell, Phys. Rev. B **29**, 2926 (1984); (b) D. Blaudez, T. Buffeteau, B. Desbat, P. Fournier, A. M. Ritcey, and M. Pezolet, J. Phys. Chem. **102**, 99 (1998).
[36] P. Royer, J. P. Goudonnet, R. J. Warmack, and T. L. Ferrell, Phys. Rev. B **35**, 3753 (1987).
[37] R. Ruppin, Surf. Sci. **127**, 108 (1983).
[38] R. G. Barrera, M. del Castillo-Mussot, G. Monsivais, P. Villaseñor, and W. L. Mochan, Phys. Rev. B **43**, 13 819 (1991).
[39] U. Kreibig and M. Vollmer, in *Optical Properties of Metal Clusters*, edited by J. Peter Toennies, Springer Series in Material Science Vol. 25 (Springer-Verlag, Berlin, 1993).
[40] U. Kreibig and L. Genzel, Surf. Sci. **156**, 678 (1985).
[41] M. Quinten and U. Kreigig, Appl. Opt. **32**, 6173 (1993).
[42] R. Ruppin, Phys. Rev. B **11**, 2871 (1975).
[43] J. M. Gérardy and M. Ausloos, Phys. Rev. B **25**, 4204 (1982).
[44] P. B. Johnson and R. W. Christy, Phys. Rev. B **6**, 4370 (1972).
[45] H. Hovel, S. Fritz, A. Hilger, U. Kreibig, and M. Vollmer, Phys. Rev. B **48**, 18 178 (1993).